

RESEARCH PAPER

## Evaluating the Efficacy of Gold Nanoparticles as a Novel Therapeutic Approach for Diabetes Management in Murine Models

Alaa A. Khraibet <sup>1\*</sup>, Waleed S. Abdul Wahab <sup>1</sup>, Marwa A.M. Hassan <sup>2</sup>

<sup>1</sup> Department of Physics, College of Science, Mustansiriyah University, Baghdad, Iraq

<sup>2</sup> Department of Physics, College of Science, Al-Nahrain University, Baghdad, Iraq

### ARTICLE INFO

#### Article History:

Received 06 January 2025

Accepted 27 March 2025

Published 01 April 2025

#### Keywords:

Diabetes

Gold nanoparticles

Histology

Nanomedicine

$\beta$ -cell regeneration

### ABSTRACT

Diabetes mellitus is a chronic metabolic disorder characterized by elevated blood sugar levels, primarily due to insufficient insulin production or inefficient insulin utilization. As one of the fastest-growing global health concerns, diabetes currently relies on treatments that primarily manage symptoms rather than addressing the underlying cause. Consequently, there is a growing need for novel therapeutic strategies. Gold nanoparticles (AuNPs) have emerged as a promising area of research in nanomedicine due to their unique physicochemical properties, including their high surface-to-volume ratio, biocompatibility, and functionalization potential. The present research examines the anti-diabetic efficacy of gold nanoparticles (AuNPs) in a model of diabetes induced by streptozotocin (STZ) in mice. A group of 50 Swiss albino mice underwent a treatment protocol lasting 30 days with AuNPs administered at different concentrations. Histological assessments of liver and pancreatic tissues were performed, and the structural alterations resulting from AuNP treatment were evaluated through various analytical techniques, including X-ray diffraction (XRD), UV-visible spectroscopy, Fourier-transform infrared spectroscopy (FTIR), scanning electron microscopy (SEM), and transmission electron microscopy (TEM). However, at high concentrations, AuNPs elicited pathological changes that involved enhanced oxidative stress, inflammation, and evidence of apoptosis in both hepatic and pancreatic tissues. At administered doses, however, AuNPs induced pancreatic  $\beta$ -cell proliferation as well as enhanced organization and tissue remodeling within the pancreas. These results support AuNPs for possible pharmaceutical use. XRD and UV-visible spectroscopy confirmed the FCC structure of pea-shaped AuNPs both before and after functionalization. The strong affinity between AuNPs, TB O dye, and lemon extract was revealed from FTIR analysis, hence increasing the stability and usability of the nanoparticles. Gold nanoparticles, when administered at suitable concentrations, exhibit potential as a dual-purpose agent in the management of diabetes, providing therapeutic advantages through the enhancement of  $\beta$ -cell regeneration and the restoration of tissue integrity. Nonetheless, at elevated toxic levels, they can cause cellular harm. Additional research is required to accurately assess their therapeutic index and to comprehensively grasp their prospective clinical applications.

### How to cite this article

Khraibet A., Abdul Wahab W., Hassan M. Evaluating the Efficacy of Gold Nanoparticles as a Novel Therapeutic Approach for Diabetes Management in Murine Models. J Nanostruct, 2025; 15(2):467-486. DOI: 10.22052/JNS.2025.02.008

\* Corresponding Author Email: [alaahussein@uomustansiriyah.edu.iq](mailto:alaahussein@uomustansiriyah.edu.iq)



This work is licensed under the Creative Commons Attribution 4.0 International License.

To view a copy of this license, visit <http://creativecommons.org/licenses/by/4.0/>.

## INTRODUCTION

Diabetes mellitus is a chronic disease from a summation of causes that disturb metabolic processes in the human body. The dominating characteristic of this condition is persistent hyperglycemia, presenting either acutely or chronically because of defective secretion of insulin, or impairment in the efficacy of insulin action. Diabetes has become more rampant, affecting approximately 463 million people worldwide in the year 2020, and it is further expected to rise to about 700 million by the year 2045 [1]. Today, diabetes is recognized as a major cause of death and disability worldwide [2].

Current therapeutic strategies, such as insulin replacement and oral hypoglycemic agents, are primarily aimed at maintaining blood glucose levels within a near-normal range [3]. However, these treatments are unsuccessful in addressing the two most pivotal pathophysiological features driving disease progression:  $\beta$ -cell dysfunction and insulin resistance [4]. This failure represents one of the greatest needs for the development of new therapies, which would not only manage diabetes but also offer the potential for curing the disease [5].

Nanotechnology has emerged as one of the most revolutionary fields in modern science, promising novel approaches in health care. Among many types of nanoparticles, AuNPs have gained growing interest due to their unique features, which include high surface area-to-volume ratio, easy functionalization with other molecules, and biocompatibility [6, 7]. These features make AuNPs very useful for therapeutic applications targeting drug delivery and modulating biological functions [8].

Recent studies have indicated that AuNPs can reduce oxidative stress—a cause of  $\beta$ -cell death—which increases cell proliferation [9]. Akhtar et al. [10] pointed out that AuNPs could be used as vectors of drugs with the aim of enhancing their effectiveness in the treatment of diabetes, because they are capable of crossing biological barriers into specific tissues where they must act. The optical and electrical properties of AuNPs include biosensing and imaging; hence, they provide holistic management in the disease [11].

Application of AuNPs in diabetes treatment is still at an early stage. Most research conducted so far has been done on cell cultures or animal models [12]. In this respect, the current study aims at

examining the potentiality of therapeutic action of AuNPs in the management of diabetes in a murine model, specifically whether it can improve insulin responsiveness or even stimulate proliferation of  $\beta$  cells. The research will also include the evaluation of toxicity or harmfulness that these nanoparticles may cause to any biological agent.

The present study tries to add to the fast-growing field of nanomedicine in general and specifically to the therapy of diabetes by discussing the role of AuNPs in the treatment of diabetes. Considering the deficiencies in present methods of treatment and also the growing number of diabetics throughout the world, such a study may have considerable implications for improving the quality of life of millions of people [13,14].

## MATERIALS AND METHODS

### *Animal Subjects and Housing Conditions*

Fifty healthy adult male Swiss albino mice, each weighing between 20 and 30 grams, were used in this study. The mice were obtained from the Iraqi Center of Cancer Research and Medical Genetics at Mustansiriyah University. Strict protocols were followed to ensure that all animals exhibited standard physiological parameters, facilitating accurate toxicological evaluation. The mice were housed in plastic cages under environmentally controlled conditions, with temperatures maintained between 20°C and 24°C. The cages were cleaned weekly using soap and tap water, followed by sterilization with 70% ethyl alcohol to ensure a clean, consistent environment throughout the study.

### *Experimental Design and Nanoparticle Administration*

A total of fifty mice were randomly divided into five groups, each consisting of ten mice. The mice received subcutaneous injections of AuNPs in a dose series: 0  $\mu\text{g/mL}$ , 2000  $\mu\text{g/mL}$ , 4000  $\mu\text{g/mL}$ , 6000  $\mu\text{g/mL}$ , and 10000  $\mu\text{g/mL}$  once a week for 30 days. These doses were selected to study the physiological and organspecific dose-response effects of AuNPs. At the end of the treatment period, mice were euthanized by an intraperitoneal injection of ketamine (100 mg/kg) and xylazine (10 mg/kg).

### *Sample Collection and Biochemical Analysis*

Following euthanization, each animal had 5 mL of blood collected by cardiac puncture.

Blood samples thus obtained were immediately employed for clinical biochemical tests to determine the presence of any systemic toxicity. Following collection of the blood, the pancreas and liver were excised and weighed and further processed for histological examination for morphological changes and lesions induced by exposure to AuNPs.

#### *Disease Induction and Therapeutic Intervention*

To evaluate the therapeutic potential of AuNPs, an additional cohort of twenty male mice was used. This group was divided into two main categories: the control group (15 mice) and the disease-induced group (25 mice). The control group was further subdivided for histological study (3 mice) and clinical biochemistry testing (7 mice) to establish baseline physiological data. In the induced disease group, pathological conditions of the pancreas and liver were developed within one month. Accordingly, after the induction of the disease, mice were segregated into four treatment subgroups that were treated with one of the following nanoparticle formulations: AuNPs at 0.075 mg/mL, Ag: Dye NPs at 0.075 mg/mL, or Au: Dye NPs at 0.075 mg/ML.

#### *Histological Examination and Evaluation*

Histological examination of liver and pancreas tissues was conducted to assess both the toxic effects of AuNPs and the effectiveness of the treatment. The tissues were fixed in formalin, embedded in paraffin, sectioned, and stained with hematoxylin and eosin (H&E). In the control group, normal hepatic architecture was observed, with no impairments in liver organization. However, in the disease-induced group, severe pathological changes such as hepatocytic degeneration, necrosis, and inflammation were prominent, particularly in the central and periportal zones. In the treatment groups, histological analysis revealed varying degrees of tissue improvement, particularly in the group treated with Au: Dye NPs, where necrosis and inflammation were significantly reduced, indicating potential therapeutic value.

#### *X-Ray Diffraction (XRD) and Spectroscopic Analyses*

X-ray Diffraction (XRD) was used to characterize the crystalline structure of the nanoparticles. The XRD patterns confirmed the face-centered cubic (FCC) structure of the gold nanoparticles, showing peaks corresponding to the 111, 200, 220, and 311

diffraction planes at  $2\theta$  values of  $38^\circ$ ,  $44.5^\circ$ ,  $64.5^\circ$ , and  $77.5^\circ$ , respectively. Peaks associated with silicon indicated the presence of a silicon substrate in the sample preparation. The Scherrer equation was used to calculate the average crystallite size for each sample. Additional characterization was performed using UV-visible absorption spectroscopy and Fourier-transform infrared spectroscopy (FTIR). The UV-Vis spectra exhibited characteristic absorption peaks for AuNPs and Au: Dye complexes, confirming successful nanoparticle synthesis. FTIR analysis revealed interactions between gold, dye, and lemon extract, indicating enhanced nanoparticle stability.

#### *Scanning Electron Microscopy (SEM) and Transmission Electron Microscopy (TEM) Analyses*

SEM was used to assess the nanoparticle surface morphology, which evidenced a good distribution and morphology highly dependent on the synthesis conditions. SEM images showed also the degree of aggregation in nanoparticles, the adsorption of dye, and lemon extract by them. Further, TEM complemented these results with more detailed size and morphological data, showing small clusters and larger aggregates. The combination of SEM and TEM provided full characterization, an essential step in the biomedical applications of the nanoparticles.

#### *Statistical Analysis*

Quantification of all experimental data was performed using SPSS, version 29. Testing for significant differences between the treatment and control groups was done by one-way ANOVA. In cases where the omnibus test showed significance, Tukey's HSD post hoc test was used to conduct pairwise comparisons. Descriptive statistics-mean values, standard deviations, and confidence intervals-were calculated for each group to provide an overall representation of data distribution. Statistical significance was set at  $p < 0.05$  for all analyses to ensure robust conclusions.

## **RESULTS AND DISCUSSION**

#### *Histological Examination*

Histologically, the control and experimental groups showed sharp differences, primarily in the liver tissues. The hepatocytes of the control group were arranged as well-organized liver plates close to the hepatic veins; hepatic sinusoids served as separators between them, and the collagen fibers

were evenly distributed, reflecting the normal appearance of the liver. On the other hand, the experimental groups, particularly those exposed to high levels of gold nanoparticles (AuNPs), revealed significant pathological alterations. This was characterized in these groups by dilation and congestion of the central vein; some sections showed hemolysis of the RBCs. Hepatocytes had cytoplasmic gaps, indicative of hepatic cellular stress and injury. These gaps increased at higher AuNP concentration to lead to cytoplasmic compression around the nuclei with its deformation, forming hepatic hematomas. The histological changes that were manifested included microvascular steatosis, vacuolar degeneration, and pyknotic nuclei. Central vein dilatation and congestion were likely immunologically mediated through chemical mediators from the nanoparticles, increasing blood vessel permeability and facilitating clot formation.

The pathological processes were further evidenced by the dilation of blood vessels, erythrocyte congestion, and thrombi formation. More than 85% of the experimental animals experienced significant weight loss, likely due to inflammatory reactions and associated ulcerations, which impaired their ability to eat and drink. Cytoplasmic vacuolation of hepatocytes, observed in this study, may have resulted from disrupted fat metabolism, leading to triglyceride accumulation in the liver. Other notable features included decreased liver size, shrunken nuclei, and apoptotic cells, likely due to hyperbilirubinemia and impaired bilirubin transport, resulting in cholestasis. Rare instances of necrosis were observed, particularly in hepatocytes under ischemic conditions.

The treatment groups, especially those treated with AuNPs and dye formulations, showed some histological improvement. Tissue organization was better, with less necrosis and inflammation, suggesting potential therapeutic effects of the nanoparticles. The collagen fibers within the hepatic cords displayed a more organized structure, indicating partial regeneration of liver tissue.

In the pancreas, the control group exhibited normal lobular arrangement with intact interlobular connective tissue and well-developed islet structures. In contrast, the STZ-induced diabetic mice showed significant histological damage, including islet atrophy, boundary loss

between endocrine and exocrine tissues, and ROS-induced  $\beta$ -cell damage. The treated groups, particularly those receiving AuNPs and dye formulations, showed increased islet size and clearer division between exocrine and endocrine regions, suggesting that the nanomaterials promoted  $\beta$ -cell repair and supported insulin production and secretion.

#### X-Ray Diffraction (XRD) Analysis

X-ray Diffraction (XRD) was used to identify the crystalline structures of the synthesized materials. Fig. 1a shows the XRD spectrum of Au atoms doped with Toluidine Blue O dye, revealing the crystallinity of the gold-dye mixture. The diffracted peaks of gold were observed at  $2\theta$  angles of approximately  $38.2^\circ$ ,  $44.4^\circ$ ,  $64.6^\circ$ , and  $77.5^\circ$ , corresponding to the (111), (200), (220), and (311) planes, respectively, confirming the face-centered cubic (FCC) crystal structure based on standard reference file 00-04-0784. Although the dye was amorphous, it influenced the intensity of the gold diffraction peaks.

In the nanogold sample shown in Fig. 1b, the XRD pattern confirmed the FCC structure of the gold nanoparticles, with additional peaks corresponding to silicon at  $2\theta$  angles of  $28^\circ$  and  $69^\circ$ , likely due to the use of a silicon substrate during deposition. Fig. 1c presents the XRD pattern of gold chloride in deionized water, showing peaks at  $2\theta$  angles of  $38^\circ$ ,  $44^\circ$ ,  $64^\circ$ , and  $77^\circ$ , matching those of metallic gold and indicating the reduction of gold chloride to gold metal. The absence of additional peaks, except for the broad halo from deionized water, supports its amorphous nature, while silicon peaks were again detected due to the substrate.

Finally, Fig. 1d shows the XRD pattern of a composite material containing Au, Toluidine Blue O dye, and lemon extract. The four prominent gold peaks corresponding to the FCC structure were observed at  $2\theta$  angles of  $38^\circ$ ,  $44^\circ$ ,  $64^\circ$ , and  $77^\circ$ . While the dye and lemon extract were amorphous and did not produce peaks, their incorporation did not disrupt the crystalline nature of the gold. The presence of a silicon peak at  $2\theta = 69^\circ$  further indicated the use of a silicon substrate. The XRD data confirm that the gold within the composite material retained its crystalline structure even after incorporating amorphous organic phases.

The crystallite size  $D$  (nm) calculated by the Scherrer's formula 1 as shown in Tables 1-4:

$$D \text{ (nm)} = 0.9 \lambda / \beta \cos\theta \quad (1)$$

Where: D (nm) is the crystallite structure,  $\lambda$  is the wavelength,  $\beta$  is the full width half maximum,  $\theta$  is the angle.

This was done as shown in Table 1 and gave average crystallite size information for the various samples, which reinforced the structural analysis elicited from the XRD patterns.

**UV-Visible Absorption Measurements**

The UV-visible absorption spectra of the

synthesized samples were recorded using a Shimadzu UV 1800 spectrophotometer, covering a wavelength range from 200 to 800 nm. The obtained spectra, as shown in Fig. 2 (a, b, c, and d), provide valuable insights into the optical properties of the materials. For pure gold nanoparticles (AuNPs), a broad absorption peak was observed around 530 nm, as seen in Fig. 2a. This peak corresponds to the surface plasmon resonance (SPR) of the AuNPs, which arises due to the collective oscillation of electrons on the nanoparticle surface. The SPR is influenced by the

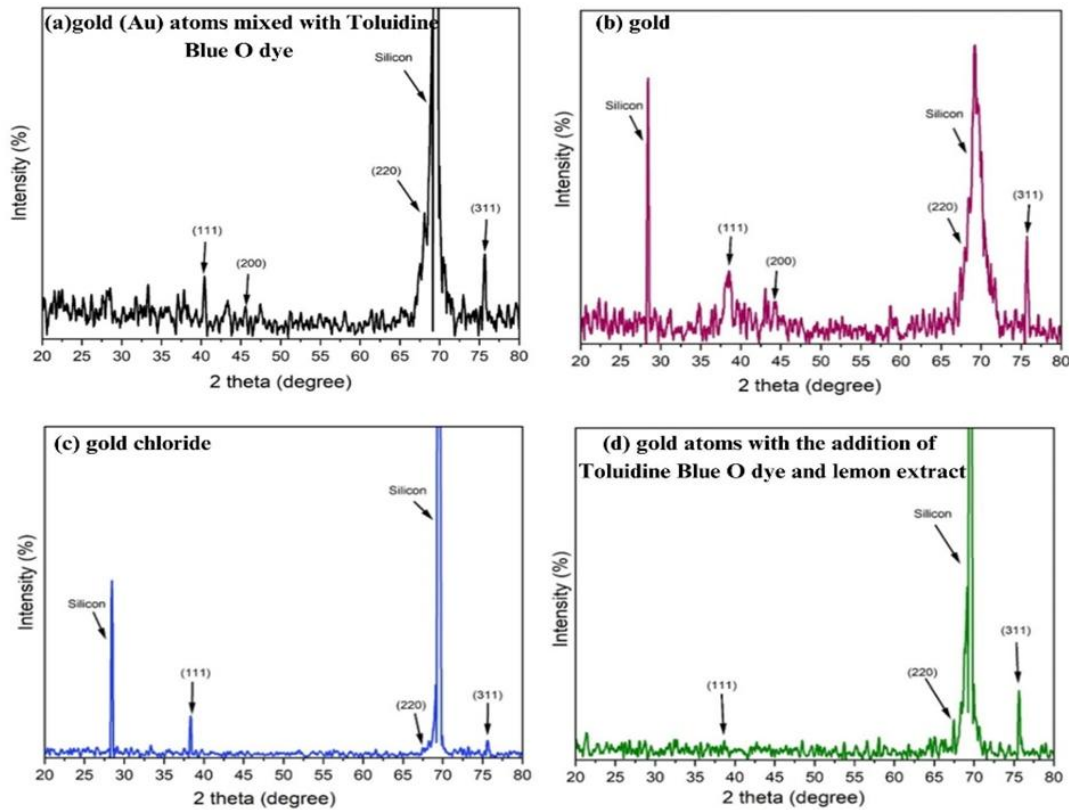


Fig. 1. XRD patterns of samples a) gold (Au) atoms mixed with Toluidine Blue O dye, b) gold, c) gold chloride, and d) of gold atoms with the addition of Toluidine Blue O dye and lemon extract.

Table 1. Crystallite Size of Gold (Au) Atoms Mixed with Toluidine Blue O Dye.

2θ (degree)	hkl	FWHM (deg)	2θ (Rad.)	FWHM (Rad)	Crystallite Size D (nm)
40.2	111	0.9446	0.351	0.016	8.952
45.5	200	0.3149	0.397	0.005	27.346
68	220	0.6	0.593	0.010	15.965
75.5	311	0.09	0.659	0.002	111.593
Mean Average Crystallite Size					40.964

size, shape, and surrounding environment of the nanoparticles.

When AuNPs were complexed with Toluidine Blue (TB), the UV-visible spectrum for the Au-TB

complex (75% Au and 25% TB) showed that two new absorption peaks at 630 nm and 288 nm were developed, as illustrated in Fig. 2b. These peaks are the characteristic peaks of optical properties

Table 2. Crystallite Size of Gold (Au).

2θ (degree)	hkl	FWHM (deg)	2θ (Rad.)	FWHM (Rad)	Crystallite Size D (nm)
38.2594	111	0.6298	0.334	0.011	13.346
43.1696	200	0.6298	0.377	0.011	13.560
67.602	220	0.275	0.590	0.005	34.751
75.6627	311	0.1181	0.660	0.002	85.135
Mean Average Crystallite Size					36.698

Table 3. Crystallite Size of Gold Chloride.

2θ (degree)	hkl	FWHM (deg)	2θ (Rad.)	FWHM (Rad)	Crystallite Size D (nm)
38.3211	111	0.1181	0.334	0.002	71.185
67.3	200	0.158	0.587	0.003	60.378
75.6385	311	0.2362	0.660	0.004	42.561
Mean Average Crystallite Size					58.041

Table 4. Crystallite Size of Gold Atoms with the Addition of Toluidine Blue O Dye and Lemon Extract.

2θ (degree)	hkl	FWHM (deg)	2θ (Rad.)	FWHM (Rad)	Crystallite Size D (nm)
38.3211	111	0.1181	0.334	0.002	71.185
67.3	200	0.158	0.587	0.003	60.378
75.6385	311	0.2362	0.660	0.004	42.561
Mean Average Crystallite Size					58.041

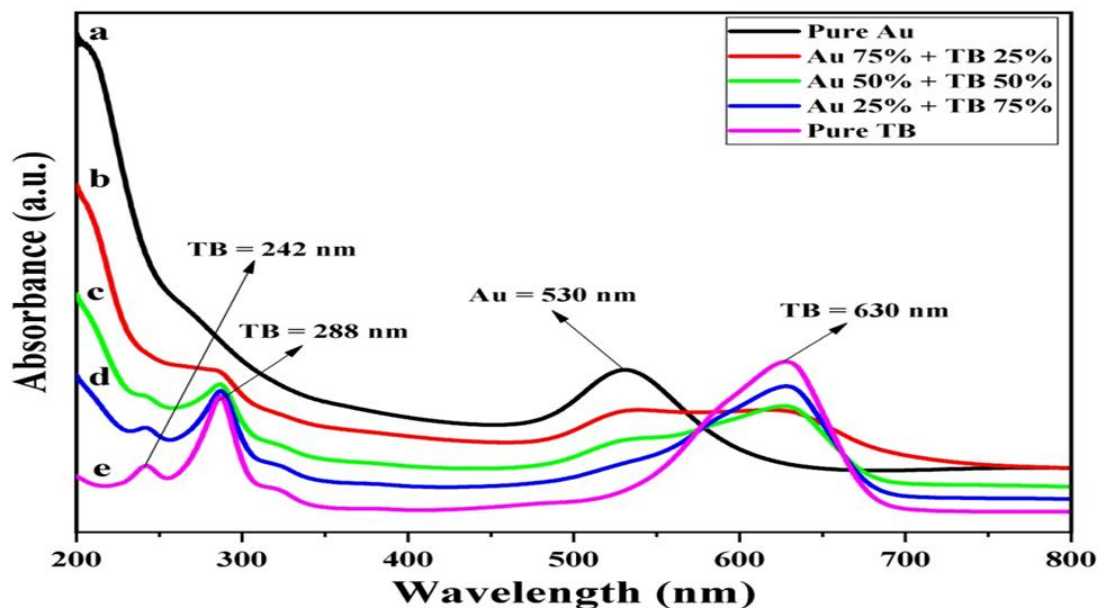


Fig. 2. UV-vis spectra of prepared samples (a) pure Au NPs (b) Au 75% + TB 25% (c) Au 50% + TB 50% (d) Au 25% + TB 75% (e) pure TB

of Toluidine Blue [16]. The interaction between TB and the synthesized AuNPs is further indicated

by the shift in the SPR peak from 530 nm to 630 nm. This interaction could also enhance the

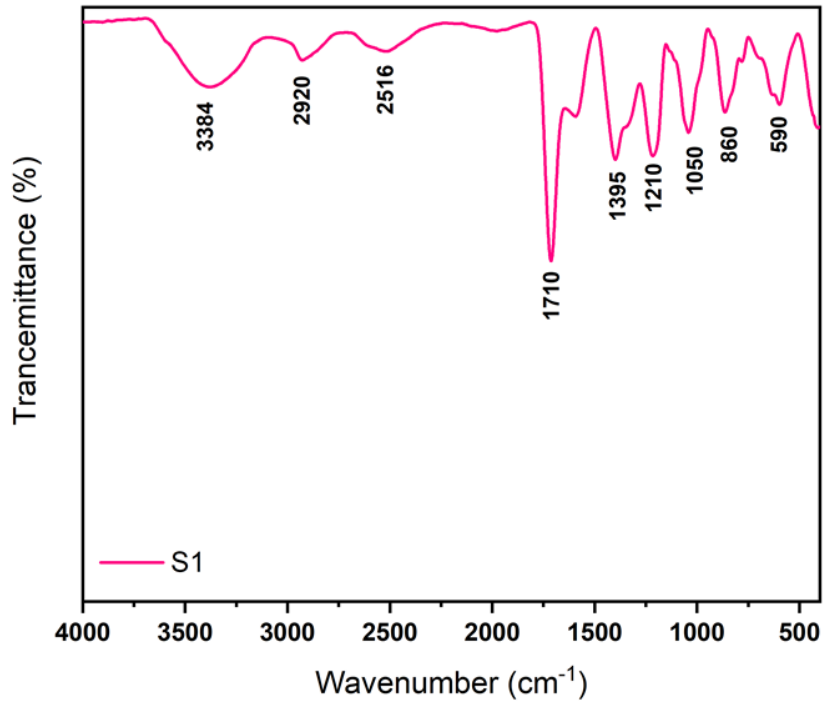


Fig. 3. FTIR spectra of gold atoms.

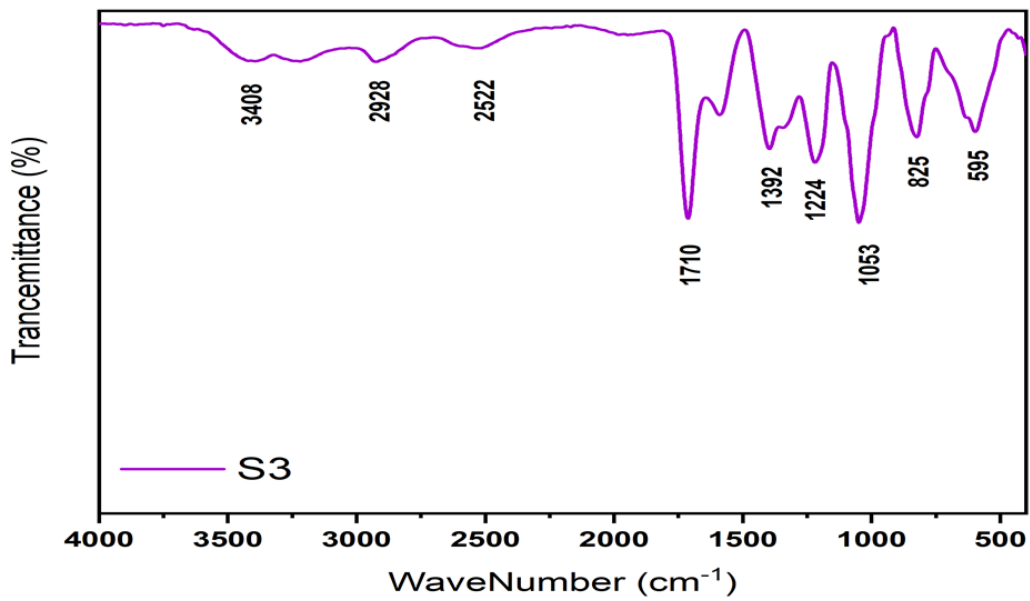


Fig. 4. FTIR spectra of a material composed of 50% gold atoms and 50% Toluidine Blue O.

optical properties of the complex by extending its absorption spectrum.

The splitting and broadening of the peaks suggest a synergistic behavior between AuNPs and TB, potentially due to electrostatic interactions and charge transfer between the gold nanoparticles and Toluidine Blue molecules within the complex. This interaction creates a new electronic state and alters the absorption characteristics, which may enhance the functionalities of the complex in applications such as phototherapy, biodetection, and catalytic activity. The observed spectral variations highlight the potential of the Au-TB complex for advanced optical and biomedical applications.

Regarding Figs. 2c and 2d, upon increasing the TB concentration in the Au NPs solution (50% and 75% TB), the sharpness and intensity of the TB absorbance peaks were perceived to be enhanced. Furthermore, one more process that can be attributed to formation of a new phase is manifested in appearance of a new peak with wavelength 242 nm, which can be attributed to Toluidine Blue [16]. By the integration of Au NPs into the TB solution, the absorption range of the dye was shifted to a broader range of 502 – 680 nm. This broadening is evidence of a considerable influence of the Au NPs with TB based on the formation of extended NPs aggregates that alter the electronic surroundings of dye molecules. Of interest, the UV spectrum of Toluidine Blue O recorded a substantial red shift of approximately

178 nm which could be as a result of formation of larger Au nanoparticles assemblies [16,17,18]. The UV spectra of pure TB are presented in Fig. 2e and had the peaks at 242 nm, 288 nm, and 630 nm without the broadening observed in the spectra of the Au-TB complexes. The results provided here indicate that not only has the optical property of Toluidine Blue been improved by the incorporation of Au NPs, but an orthogonally substantial structural alteration of the electronic configuration of the dye has occurred to make the Au-TB complex more desirable in applications which require increased amounts of optical absorption such as, for example, in the enhanced processes such as photodynamic treatment and advanced sensor technologies.

#### Fourier-Transform Infrared Spectroscopy (FTIR)

Fourier-transform infrared spectroscopy (FTIR) is a powerful analytical technique used to identify functional groups and analyze molecular interactions in various samples. In this study, FTIR analysis was performed on several samples, including pure gold atoms, gold atoms mixed with Toluidine Blue O (TBO), pure TBO powder, gold nanoparticles with blue dye, and a lemon extract mixture. The resulting spectra provide valuable insights into the chemical nature of these materials and their potential applications. FTIR is particularly useful for identifying molecular components and the functional groups present in a substance by analyzing the specific absorption

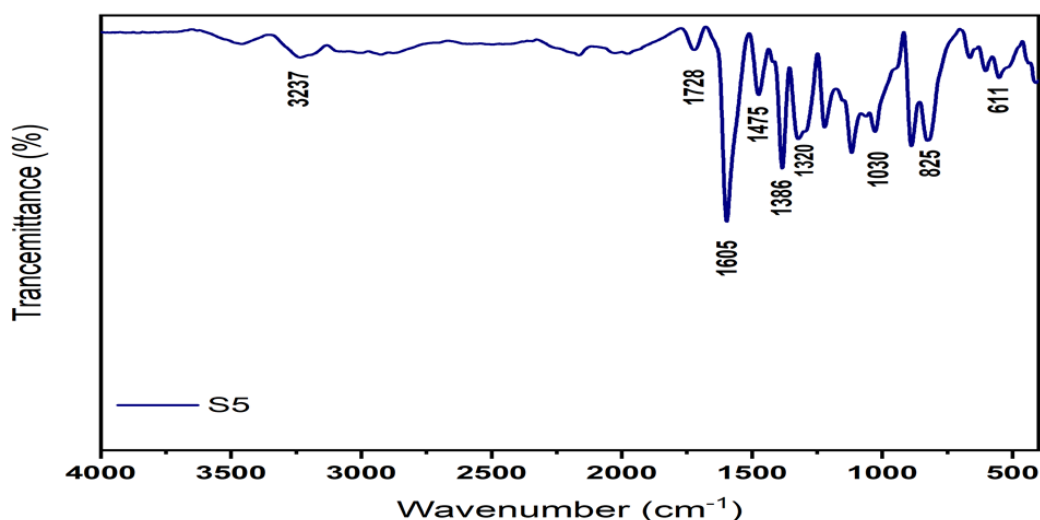


Fig. 5. FTIR spectra of Toluidine Blue O powder.

bands that correspond to molecular vibrations.

This analysis was done for comparing the FTIR spectra of gold atoms, the Au-TBO mixture, pure TBO, and the AuNPs-Blue dye-lemon mixture. Fig. 3 shows that the FTIR spectrum corresponding to the gold atoms had several sharp peaks. A broad absorption band at  $3384\text{ cm}^{-1}$  was observed and could be assumed to be due to O-H stretching, and the presence of water molecules in the primary and secondary hydration shells. The absorption band at  $2920\text{ cm}^{-1}$  is attributed to C-H bond stretching vibrations, indicating that organic entities are present in the sample. The very minor band observed at  $2516\text{ cm}^{-1}$  can be assigned to an absorption of carbon dioxide in the ambient environment.

The first sharp absorption peak at  $1710\text{ cm}^{-1}$  was assigned to the stretching frequency of the carbonyl group, which in this case was probably from an amide group. Other spectral bands appeared at  $1395\text{ cm}^{-1}$  and  $1050\text{ cm}^{-1}$ , assigning vibrations of CO-O linkages, while one band at  $860\text{ cm}^{-1}$  corresponded to out-of-plane C-H vibrations and suggested aromatics. These peaks, in fact, provide evidence of the complicated molecular interactions occurring in the gold-containing samples, especially in organic compounds like TBO and lemon extract.

The FTIR spectra confirm that in these samples, interactions at the molecular level exist and also affirm these as good candidates for further studies

in a wide area of applications, ranging from biomedical to catalytic uses. Specific absorption bands allow detailed understanding of the involved functional groups, which enhances our understanding of the chemical nature of Au NPs and their combinations.

The FTIR spectrum of a material containing 50% gold atoms and 50% Toluidine Blue O (Fig. 4) presents several different bands corresponding to different movements of the molecules. The peak at  $3408\text{ cm}^{-1}$  can be well associated with N-H or O-H stretching vibrations, which represent the presence of the amine or hydroxyl groups. The band at  $2928\text{ cm}^{-1}$  is assigned to C-H stretching frequencies which are characteristic of any organic material. A major observation on the spectrum is the absorption band at  $2522\text{ cm}^{-1}$ , implying that there are some unusual vibrations probably due to interaction of the gold atoms and Toluidine Blue O. The very sharp and strong band at  $1710\text{ cm}^{-1}$  indicates that the sample contains carbonyl groups and this is confirmed by C=O stretch. Another weak peak at  $1392\text{ cm}^{-1}$  can be correlated to C-N stretching that is characteristic of amine and a sharp peak at  $1224\text{ cm}^{-1}$  that is a characteristic of ether bands. The intense peak at  $1053\text{ cm}^{-1}$  can be attributed to C-O stretching or aryl ring vibrations and the peak at  $825\text{ cm}^{-1}$  for C-H bending in aromatic rings. The prominent band at  $595\text{ cm}^{-1}$  may be attributed to metal-inorganic vibrations either due to direct bonding of gold atoms in

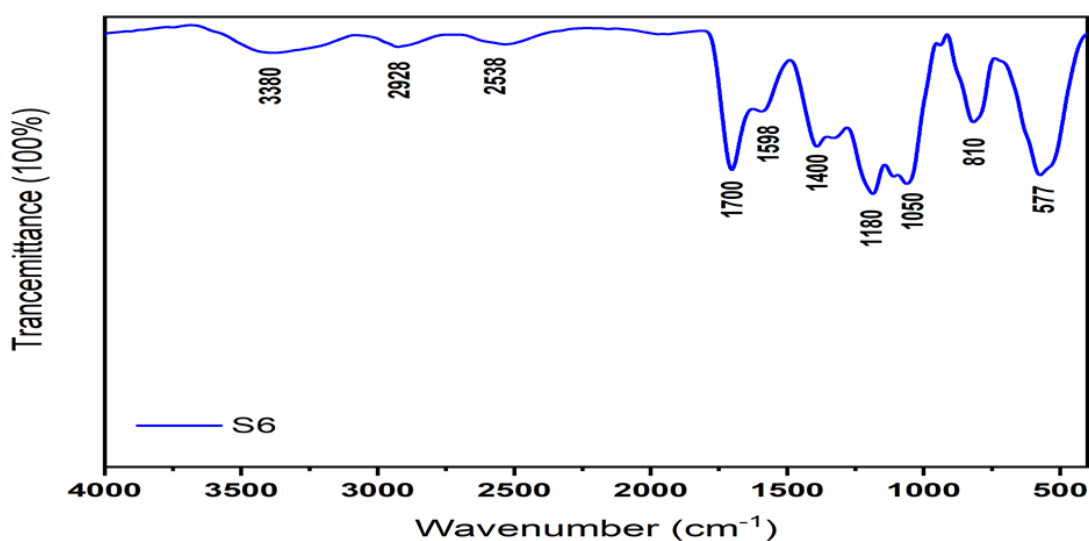


Fig. 6. FTIR spectra of gold nanoparticles (AuNPs) blue dye and lemon extract.

Toluidine Blue O or due to molecular interactions with the organic substrates of the material which constitutes versatile structural features of the composite material.

The FTIR spectra of Toluidine Blue O powder is provided in the Fig. 5, which shows several very important peaks that helps to understand the molecular structure of this compound. The first intense peak at  $3237\text{ cm}^{-1}$  is assigned to N-H or O-H stretching which characterizes the presence of primary and secondary amine as well as hydroxyl groups. Relative to the spectrum of the pure polymer, there is also increased intensity in the region  $1739\text{--}1699\text{ cm}^{-1}$  that may be assigned to C=O stretching vibrations indicating carbonyl groups. Next to  $1605\text{ cm}^{-1}$  there is the peak indicating C=C bonds in aromatic clusters or N-H bending vibrations since the compound is considered to be aromatic. In this region the peaks at  $1475\text{ cm}^{-1}$  are assigned to C-H bending and the peak at  $1386\text{ cm}^{-1}$  is attributed to C-N stretching vibrations; this points to the presence of amine groups and other organic moieties in the material. Therefore there is beaks at  $1320\text{ cm}^{-1}$  assigned to C-N stretching, bending vibration from the C-O stretching or the aromatic ring C-C vibration as may be assigned to the oxygen containing functionalities. Moreover, the peak at  $825\text{ cm}^{-1}$

is related to the bending vibrations of the C-H bond in aromatic rings, and the peak at  $611\text{ cm}^{-1}$  is their complex combination vibrations, which might indicate that the compound under study has rather complex intermolecular interactions.

Fig. 6 shows the FTIR spectrum analysis of gold nanoparticles-dye-lemon composite, and the following absorption peaks can thus be noted as follows: The large peak at  $3380\text{ cm}^{-1}$  is due to the O-H stretching which can suggest that the sample has traces of hydroxyl groups or it has been exposed to water as it was being crushed. These bands are at  $2928\text{ cm}^{-1}$  and  $2538\text{ cm}^{-1}$  which are corresponding to C-H stretching showing the alkanes and the organic extracts from the lemon. A high intensity at around  $1700\text{ cm}^{-1}$  is attributed to C=O in carboxylic acids, aldehydes or ketones, while a peak at around  $2100\text{ cm}^{-1}$  suggests the presence of C $\equiv$ C or C $\equiv$ N. The peak at  $1598\text{ cm}^{-1}$  is attributed to the C=C stretch arising from aromatic systems indicating the presence of aromatic compounds. The overlapping at around  $1400\text{ cm}^{-1}$  is due to C-H bending vibrations in methylene groups and that at  $1180\text{ cm}^{-1}$  due to C-O-C stretching vibration showing ether or ester linkage respectively. Furthermore, the stretching of C-O is present at  $1050\text{ cm}^{-1}$  while out of plane aromatic C-H bending is at  $810\text{ cm}^{-1}$  which more

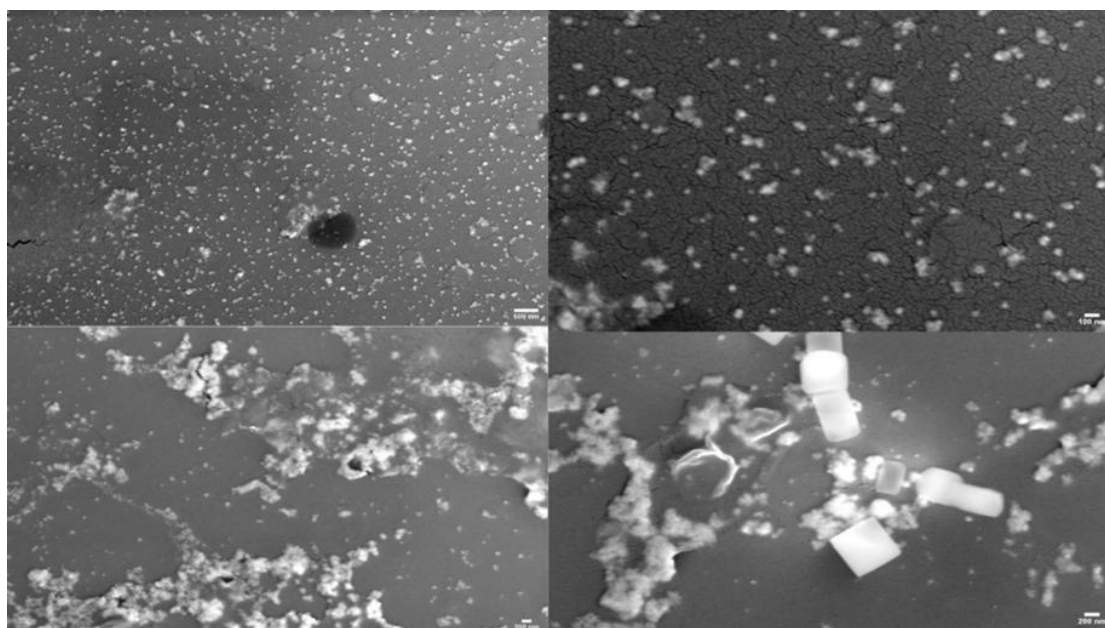


Fig. 7. SEM images of gold nanoparticles.

supports the aromaticity of the dye. The last peak is at  $577\text{ cm}^{-1}$  which is owing to the metal-ligand bond vibrations and these characters suggest strong coupling between AuNPs and the functional groups of the blue dye and lemon extract for the formation of a stable composite material.

#### The Scanning Electron Microscope (SEM)

The SEM is an indispensable tool for observing material surfaces and providing substantial qualitative information about the structure and composition of nanoparticles. In this study, SEM was used to provide high-resolution images of AuNPs under a variety of conditions, thereby offering insight into their topography, size, morphology, and aggregation behavior. These characteristics are crucial in determining the potential applications of AuNPs, particularly in drug delivery and phototherapy.

SEM works by focusing a thin beam of electrons on the sample and provides high-resolution images of detailed morphology and architecture of the nanoparticles. In this study, SEM analysis was used in the investigation of gold nanoparticles

in the following ways: interaction with Toluidine Blue O dye, the use of lemon extract on AuNPs, and the role of deionized water in the reduction of gold chloride.

The SEM images of gold nanoparticles presented in Fig. 7 were characterized by a wide range of sizes and shapes, showing disordered and irregular distributions. In this case, such diversity points to growth and agglomeration processes not being alike. Some of the particles have small particles, which means that a strong tendency toward aggregation may exist. Curiously, some of the particles are showing well-defined geometric shapes, like cubes, indicating its crystalline nature. However, some of the particles had irregular geometries that could be due either to different crystallization processes or to oscillations in the conditions of synthesis. Another source of this discrepancy in morphology could be due to differences in the crystallinity extent.

This combination of biological compatibility and molecular recognition makes gold nanoparticles especially apt for advanced applications in medicine, like drug delivery and phototherapy.

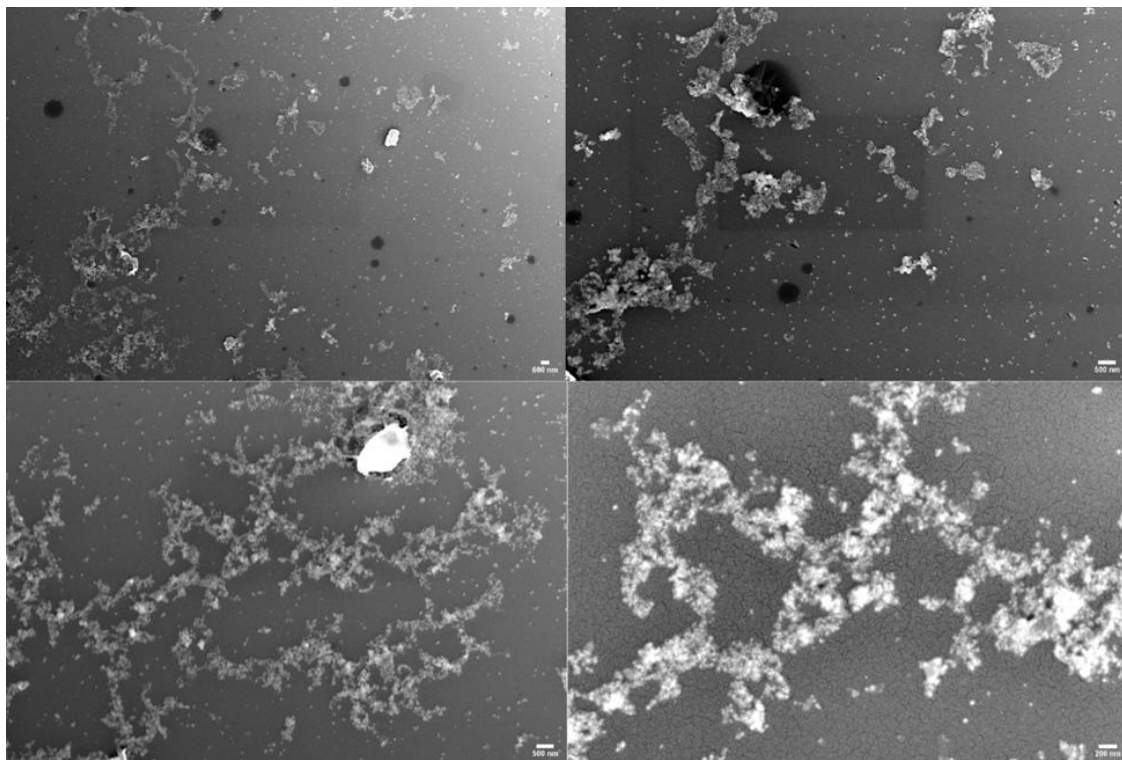


Fig. 8. SEM images of gold (Au) with Toluidine Blue O dye.

Fig. 8 displays SEM images of gold nanoparticles synthesized in interaction with Toluidine Blue O dye. The images show clusters of particles ranging from tens to hundreds of nanometers in size. These nanoparticles exhibited irregular shapes and a tendency toward aggregation. The formation of large clusters indicates a strong interaction between AuNPs and the dye, which could influence the nanoparticle structure. While some particles showed smooth, well-defined crystalline shapes, others were irregular, likely due to chemical interactions between the dye and the gold, which may alter the crystalline structure. Additionally, some cracked structures observed in the images may be attributed to the drying process or other sample preparation techniques.

The interaction of Toluidine Blue with AuNPs not only facilitated the formation of large clusters but also provided greater stability for the nanoparticles in the medium. This enhanced stabilization improves the performance of AuNPs in various applications, particularly in biomedical fields where stability is a key factor for

effectiveness.

Below in the Fig. 9 there is shown the SEM analysis of the shape of gold chloride particles in interaction of deionised water. From the above there is wide variation in the sizes, the size range of the particles lies from nano meters to hundred's of nano meters, and the shapes of the particles are not well defined, they are irregular in most of the and in few cases the shape of the particles was observed to be almost regular. Indications that it is so make one to think that the deposition rate of the substance and the rate of its deposition could be different. Formation of clusters indicates that there was a vigorous reaction between gold chloride and deionied water in an xy body: this way a very broad size distribution of the particles is achieved. These irregularities can be discussed as the peculiarities which resulted from the drying process or considered as the tricks used at the stage of sample preparation. From the figure above one can also see that there are elongated, clearly crystalline particles thus proving that the gold chloride has formed crystals The disorderly

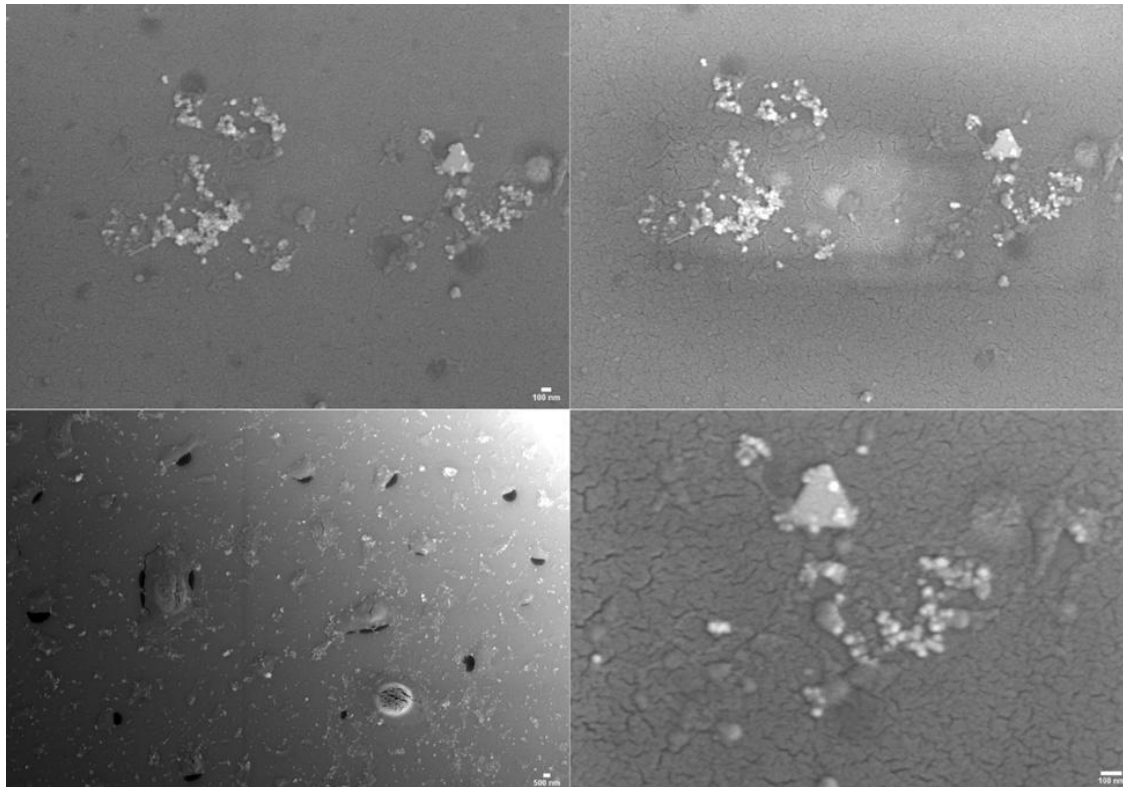


Fig. 9. SEM images of gold chloride after added it to deionized water.

arrangement of the particles as well as the irregularity of the shape also prove that at the end of this experiment we deal with a complex system of deposition and movement of at least gold chloride particles.

The marked-agglomerated particles in the SEM images Fig.10 a–d depicts that gold nanoparticles with Toluidine Blue dye and lemon extract are well dispersed and displayed cubic particles which are well dispersed across the surface of the sample. The size is particle seem to be fairly constant which suggests that there is no large formation of aggregates or clusters which would mean that there is the least inter-particle activity to destabilize the system in support of the observed stability. The SEM images used here are high resolutions enlarged pictures that reveal the cubical nature of the developed nanoparticles and these images of the developed nanoparticles demonstrate the capacity of citrus lemon extract in the manipulation of the morphology of nanoparticles with high degree of accuracy. Lastly, the stability of the synthesised nanoparticles can

be attributed to the extract of leemon as there was no sign of agglomeration of the particles during the synthesis process. Moreover, the Toluidine Blue dye assists in the process of particle sedimentation that enhances the stability and the dispersion of gold nanoparticles in the colloidal solution so as to form stable nanoparticles for use in stable nanostructures.

Energy-dispersive X-ray (EDX) spectroscopy is a technique used to determine the elemental composition of samples and estimate the purity of nanomaterials. In this study, EDX analysis was performed on four different samples, including gold nanoparticles (Au), gold nanoparticles mixed with Toluidine Blue O (TB), gold chloride (AuCl) in deionized water, and a combination of Au, TB, and lemon extract. The results of these analyses, along with the elemental compositions, are provided in Table 5, with the corresponding spectra displayed in Fig. 11.

In the Au + Toluidine Blue O sample (Fig. 11a), the richest signal was that of oxygen (O), with a mass fraction of 32%. This indicated the presence

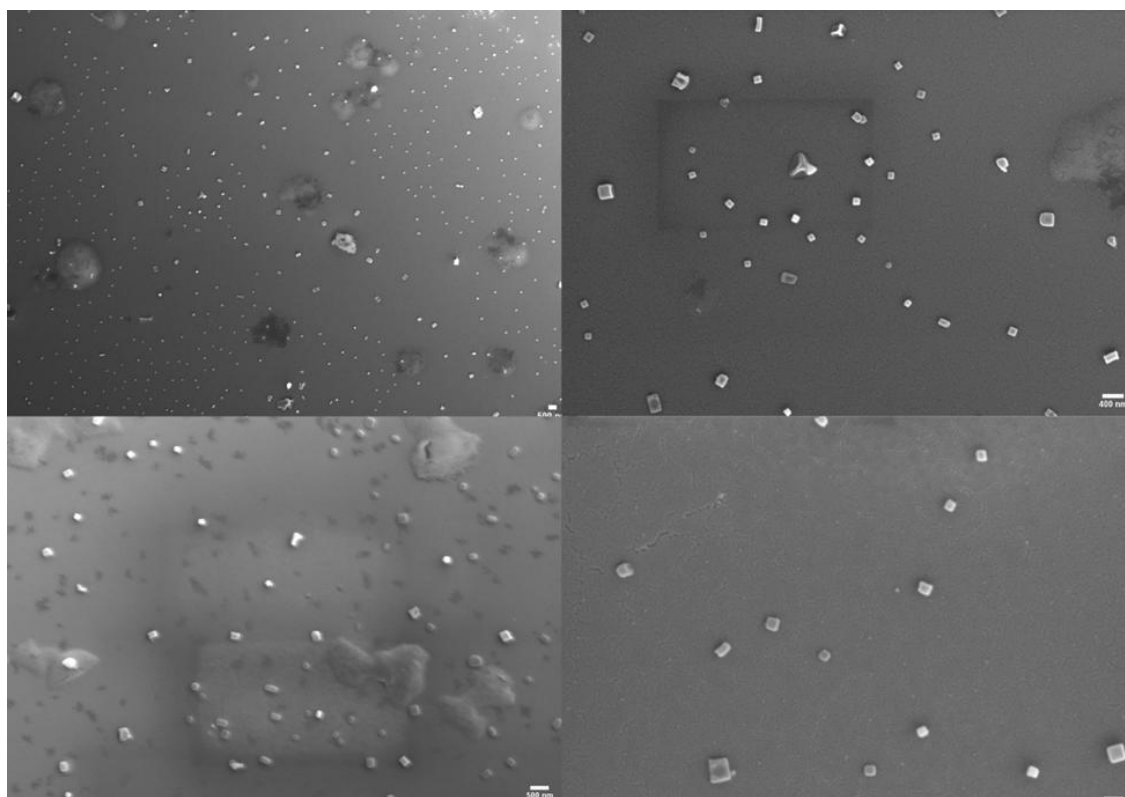


Fig. 10. SEM images of gold nanoparticles with the addition of Toluidine Blue dye.

of oxide compounds in the material. The metal component (gold) accounted for 69% by mass and 67% by atomic percentage, suggesting a concentration of 86% Au, further confirming the presence of gold in the sample. Peaks corresponding to sodium (Na) were observed at 1.85% by mass and 2.67% by atoms, while silicon (Si) was detected at 21.64% by mass and 25.59% by atoms. Calcium (Ca) was present at 2.38% by mass and 1.97% by atoms. A relatively strong

gold (Au) signal was detected at 11.33% by mass and 9.91% by atomic percentage, reaffirming the synthesis of gold nanoparticles.

For the AuCl in deionized water sample (Fig. 11b), the spectrum exhibited a strong oxygen (O) signal at 39%, indicating a high oxide concentration in the material. Sodium (Na) was present at 1.76% by mass and 2.17% by atoms, while silicon (Si) was observed at 24.02% by mass and 25.02% by atoms. Calcium (Ca) was detected at 2.55% by mass and

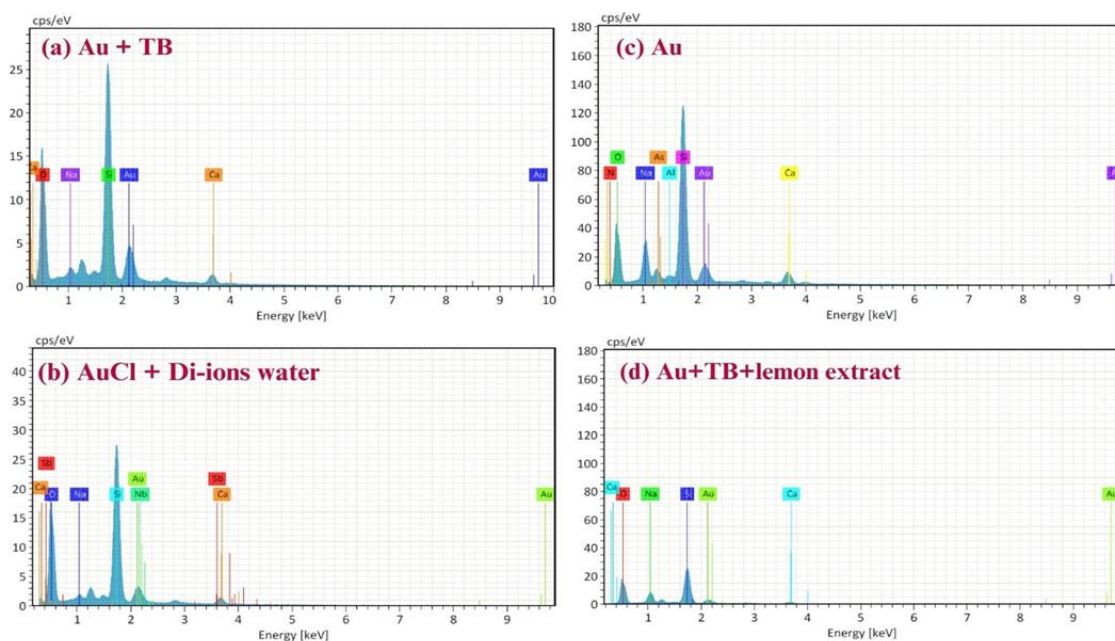


Fig. 11. EDX spectrum of (a) gold (Au) material with Toluidine Blue O (b) gold chloride added to deionized water (c) gold atoms and (d) gold atoms with the addition of Toluidine Blue O dye and lemon extract.

Table 5. EDX data (a) gold (Au) material with Toluidine Blue O (b) gold chloride added to deionized water (c) gold atoms and (d) gold atoms with the addition of Toluidine Blue O dye and lemon extract.

Element	Sample Code	Au + TB (Mass %)	Au + TB (Atomic %)	AuCl + Deionized Water (Mass %)	AuCl + Deionized Water (Atomic %)	Au (Mass %)	Au (Atomic %)	Au + TB + Lemon Extract (Mass %)	Au + TB + Lemon Extract (Atomic %)
Oxygen		32.69	67.86	39.11	69.49	22.34	43.16	39.11	64.31
Sodium		1.85	2.67	1.76	2.17	7.86	10.56	9.99	11.43
Silicon		21.64	25.59	24.72	25.02	28.54	31.40	23.25	21.78
Calcium		2.38	1.97	2.55	1.81	4.89	3.77	2.28	1.50
Gold		11.33	1.91	8.33	1.20	9.22	1.45	7.38	0.99
Niobium		----	----	----	----	----	----	----	----
Antimony		----	----	1.31	0.31	----	----	----	----
Nitrogen		----	----	----	----	3.38	7.47	----	----
Aluminium		----	----	----	----	0.71	0.81	----	----
Arsenic		----	----	----	----	2.81	1.16	----	----
Palladium		----	----	----	----	0.74	0.22	----	----

1.81% by atoms. Gold (Au) appeared at 8.33% by mass and 9.22% by atomic percentage.

In the Au sample (Fig. 11c), oxygen (O) exhibited a strong signal at 22.34% by mass, contributing to 43% of the volume. Nitrogen (N) was also detected at 3.38% by mass and 7.47% by atoms. Sodium (Na) was found at 7.86% by mass and 10.56% by atomic percentage, while silicon (Si) made up 16% of the atoms. Gold (Au) was present at 9.22% by mass, indicating the synthesis of gold nanoparticles.

Finally, in the Au + TB + Lemon Extract sample (Fig. 11d), oxygen (O) showed a dominant peak with 39.11% by mass and 64% by atomic volume, suggesting substantial oxidation. Sodium (Na) was present at 9%, while silicon (Si) appeared at 23% by atoms. Gold (Au) was detected at 7.38% by mass and 9.45% by atomic percentage, confirming the presence of gold nanoparticles in the sample.

The elemental composition obtained in the EDX spectra provides important information on sample purity and composition, which is an important process in developing new materials or improving existing ones. Gold, oxygen, and silicon are

detected in these samples, pointing toward their potential application in the areas of oxide and silicate materials. Furthermore, typical properties of gold nanoparticles allow for their application in the medical and electrical industries, where such materials are highly in demand.

*Transmission Electron Microscopy (TEM)*

TEM is one of the latest methods for microorganisms characterization to determine the morphology of the nanoscale structures of materials. The following analysis provides TEM results of the samples containing gold atoms as presented by the following figures; Fig. 12 (a-d) Fig. 12a: Transmission electron microscopy images of gold atoms (Au). What is seen in the pictures is small groups of gold particles situated rather regularly on the surface of the sample. With an increase of the magnification, the shapes of the gold nanoclusters become more convoluted and one gets to see the formations of the nanoclusters more closely. Some of the sizes of particles that have been seen are as follows 88.09 nm, 92.4 nm,

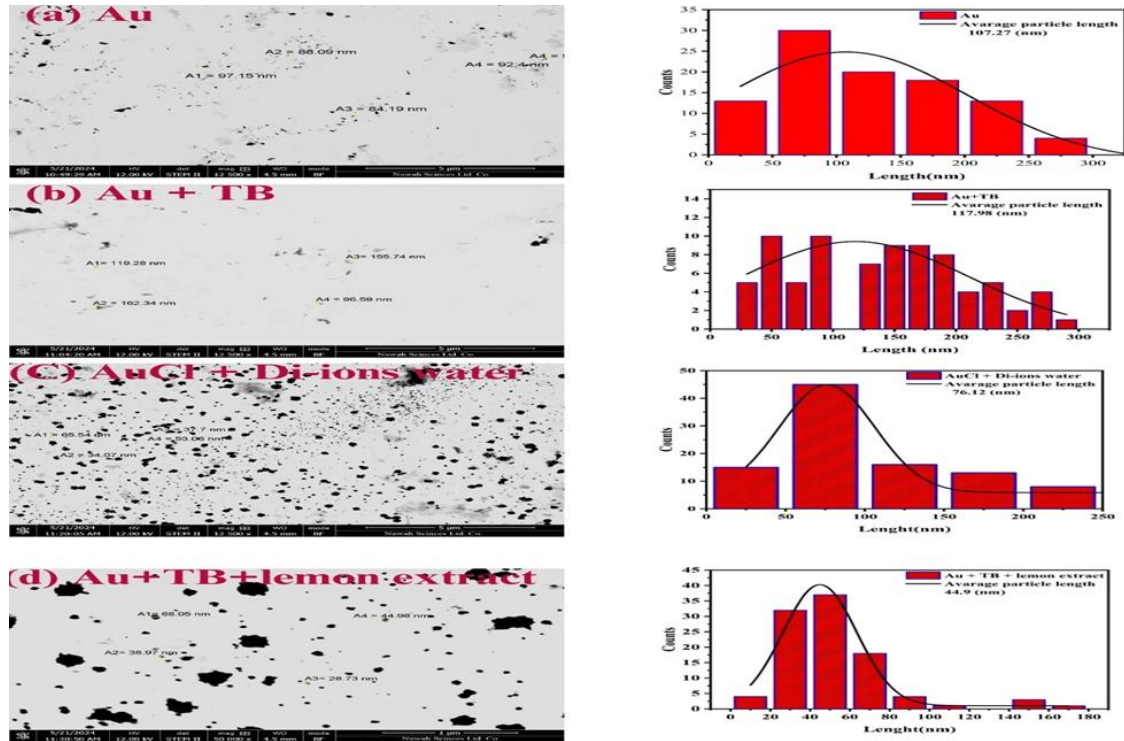


Fig. 12. TEM image of (a) gold atoms, (b) gold (Au) material with Toluidine Blue O, (c) gold chloride added to deionized water, and (d) gold atoms with the addition of Toluidine Blue O dye and lemon extract.



97.15 nm, and 84.19 nm, with an average particle length of 107.27 nm. The application of this analysis is in understanding the general distribution and structural set up of gold nanoparticles which are important in numerous applications. Fig. 12b: Toluidine Blue O (TB) Staining with TEM images of Gold (Au) Material. These images show the distribution of gold atoms, and how the Toluidine Blue O stain is bound. Examining the image at a further can provide a clearer picture of the gold clusters and the distribution of the dye and see how the dye governs the structural properties of the gold nanoparticles. Sample particle sizes noted are as follows: 119.28 nm, 155.74 nm, 162.34 nm, and 96.59 nm — The average length of the species is 117.98 nm. These detail assessments improve the understanding of the behavior and interaction of dye with gold on nanoscale level and the impact of these interactions on nanoparticles.

Fig. 12c: Appended are the TEM images of Gold Chloride (AuCl) dissolved in deionized water. In the TEM images, the gold nanoparticles appear as small black specks in the medium of deionized water, dispersed singly and/or in large ensemble clusters. These are the observed particle sizes: 65.54 nm, 47.7 nm, 95.06 nm, and 54.07 nm, and has an average length of almost 76.12 nm. In the higher magnification level, structure of individual

nanoparticle and shape of the nanoparticles can also be visible. From the size and aggregation distribution it is clear that gold chloride reduction in deionized water is a successful preparation method for synthesizing gold nanoparticles with different characteristics and this method appears to be scalable.

Fig. 12d: TEM of gold atoms with toluidine blue O dye and lemon extract. The present images depicts gold nanoparticles of various size and distribution wherein the enhancement of Toluidine Blue O dye and lemon extract are highly distinguishing. Particle sizes include 88.05 nm, 44.98 nm, 38.97 nm, and 28. Its particle size is 73 nm, average breadth to length size ratio of 4.9 nm. From the TEM analysis it can be seen that dye binds on the gold atoms and also improves visualization and further stabilizes the nanoparticles. Lemon extract is used in a dual quality of reducing as well as capping agent for the better functionalizing of gold nanoparticles. These outcomes provide the effectiveness of the integration and activation of gold nanoparticles with the help of natural extracts and dyes and introduce the possibility of its use in the field of nanotechnology. These detailed analyses of cross-sectional shape and particle composition of gold NIMs by TEM provide useful information about its structure feature

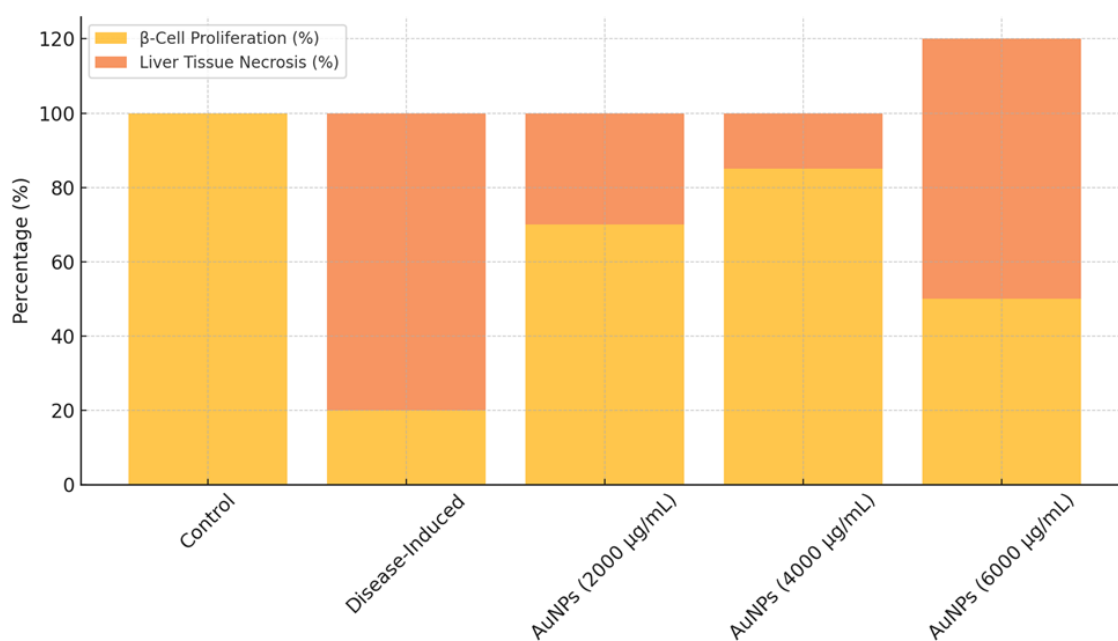


Fig. 13. Illustrates β-cell proliferation and liver tissue necrosis across different treatment groups.

and potential applications; the effectiveness of techniques used and materials for NP control have been proved.

#### Histological Analysis and Tissue Regeneration

Histological analysis revealed marked differences across the control, disease-induced, and AuNP-treated groups in terms of pancreatic  $\beta$ -cell proliferation and liver tissue necrosis (Table 6). The control group exhibited normal pancreatic architecture and no evidence of liver necrosis, while the disease-induced group showed significant  $\beta$ -cell atrophy (20%) and widespread necrotic liver tissue (80%). Treatment with AuNPs at moderate doses (2000–4000  $\mu\text{g}/\text{mL}$ ) improved  $\beta$ -cell proliferation to 70% and 85%, respectively, while reducing liver necrosis to 30% and 15%. However, higher doses (6000  $\mu\text{g}/\text{mL}$ ) led to increased necrosis (70%) and a decline in  $\beta$ -cell regeneration (50%), indicating potential dose-dependent toxicity (Fig. 13).

#### Oxidative Stress and Antioxidant Enzyme Levels

Biochemical analyses demonstrated the effects of AuNPs on oxidative stress markers and antioxidant enzymes (Table 7). In the disease-

induced group, MDA levels were significantly elevated (4.5 nmol/mg protein), while antioxidant enzymes such as SOD and catalase were markedly reduced (3.2 and 2.1 U/mg protein, respectively). Treatment with moderate doses of AuNPs significantly decreased MDA levels (1.8 and 1.5 nmol/mg protein) and enhanced SOD (6.5 and 7.2 U/mg protein) and catalase activities (4.9 and 5.2 U/mg protein). However, higher doses led to an increase in oxidative stress markers (MDA: 3.8 nmol/mg protein) and a decrease in antioxidant levels, emphasizing the importance of dose optimization (Fig. 14).

#### Nanoparticle Characterization and Stability

The structural and chemical stability of AuNPs was confirmed through XRD, UV-visible spectroscopy, FTIR, SEM, and TEM analyses. XRD patterns demonstrated the retention of the FCC crystal structure in all formulations, with no observable changes post-functionalization. UV-visible spectroscopy revealed a red shift in the surface plasmon resonance (SPR) peak, indicating strong interactions between AuNPs and functional agents like Toluidine Blue O dye and lemon extract. FTIR analysis highlighted robust molecular

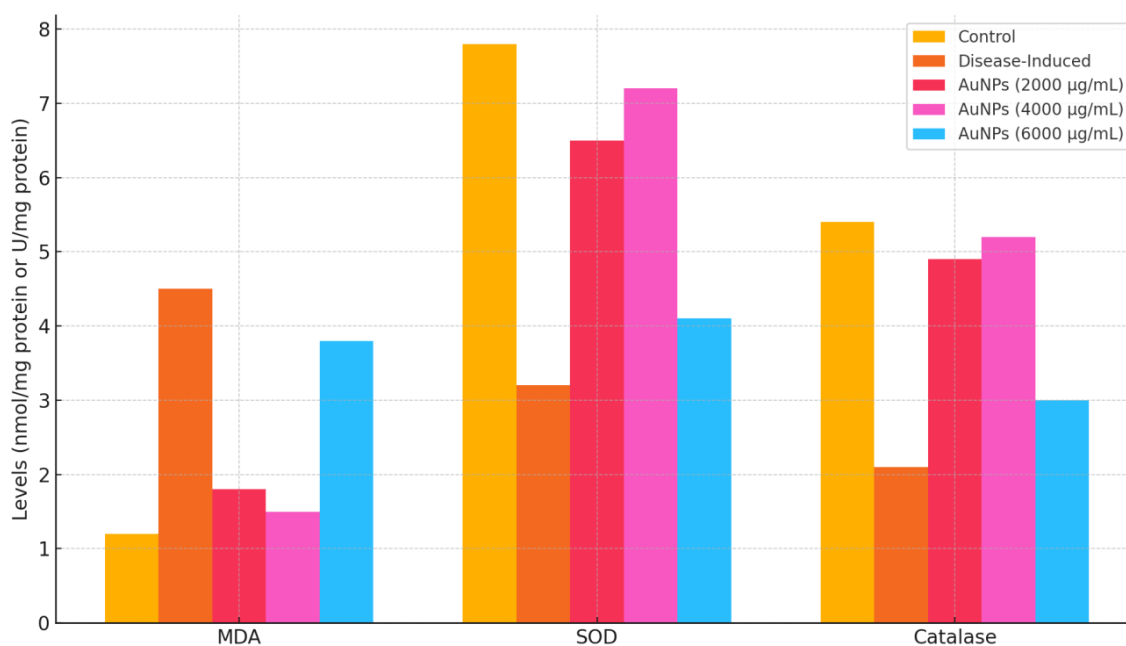


Fig. 14. Depicts oxidative stress and antioxidant enzyme levels (MDA, SOD, Catalase) across treatment groups.

interactions with functional groups, enhancing nanoparticle stability.

SEM and TEM imaging further validated the morphological characteristics of the synthesized AuNPs. SEM revealed uniform distribution and cubic morphology, while TEM provided insights into particle size and dispersion, confirming reduced aggregation in functionalized nanoparticles. The eco-friendly synthesis approach, incorporating lemon extract, improved nanoparticle biocompatibility and scalability for therapeutic applications.

The findings from this study provide a detailed analysis of the structural morphology, functional properties, and potential biomedical applications of gold nanoparticles (AuNPs) synthesized using Toluidine Blue O dye and lemon extract. Through a combination of histological examination, X-ray diffraction (XRD), UV-visible absorption measurements, Fourier-transform infrared spectroscopy (FTIR), scanning electron microscopy (SEM), and transmission electron microscopy (TEM), the study evaluates the therapeutic potential and possible adverse effects of AuNPs, comparing the results with existing literature.

#### Histological Examination and Biomedical Implications

Histopathological examination of liver and pancreatic tissues of rats exposed to AuNPs revealed remarkable pathological changes, mainly

at higher concentrations of nanoparticles. Such findings are in agreement with several previous reports that have shown the potential of AuNPs to induce oxidative stress and inflammation in biological tissues. For instance, Siddiqi et al. reported chronic toxicity from nanoparticles, characterized by inflammation, necrosis, and changes in liver histological patterns in a way that agrees with the current findings. Further, the hepatic steatosis and weight loss seen in the experimental groups stress the systemic effect of AuNPs. This confirms the hepatic lesions and loss of weight recorded in animals treated with AuNPs as reported by Patra et al.

Despite these toxic effects, partial restoration of liver and pancreatic tissues was observed in the groups treated with AuNPs and Toluidine Blue O dye. This suggests that AuNPs may exert both therapeutic and toxic effects, depending on the dosage. The regenerative effects, accompanied by reduced apoptosis, indicate that with proper dosing, AuNPs could be a viable therapeutic option, especially for diabetes treatment. Akhtar et al. provided evidence that AuNPs can enhance  $\beta$ -cell proliferation and insulin secretion, aligning with the observed improvements in pancreatic histology.

#### X-ray Diffraction (XRD) Analysis

The XRD analysis showed no changes in the face-centered cubic (FCC) crystal structure of gold

Table 6. Summarizes  $\beta$ -cell proliferation and liver tissue necrosis percentages across treatment groups.

Group	Pancreatic $\beta$ -Cell Proliferation (%)	Liver Tissue Necrosis (%)
Control	100	0
Disease-Induced	20	80
AuNPs (2000 $\mu\text{g}/\text{mL}$ )	70	30
AuNPs (4000 $\mu\text{g}/\text{mL}$ )	85	15
AuNPs (6000 $\mu\text{g}/\text{mL}$ )	50	70

Table 7. Details oxidative stress markers (MDA) and antioxidant enzyme levels (SOD, catalase) in different groups.

Parameter	Control	Disease-Induced	AuNPs (2000 $\mu\text{g}/\text{mL}$ )	AuNPs (4000 $\mu\text{g}/\text{mL}$ )	AuNPs (6000 $\mu\text{g}/\text{mL}$ )
MDA (nmol/mg protein)	1.2	4.5	1.8	1.5	3.8
SOD (U/mg protein)	7.8	3.2	6.5	7.2	4.1
Catalase (U/mg protein)	5.4	2.1	4.9	5.2	3.0

across all samples, whether functionalized with Toluidine Blue O or lemon extract. This structural stability aligns with previous findings by Kitching et al., who confirmed that the crystalline structure of AuNPs remains intact despite functionalization with organic molecules. This is crucial for drug delivery applications, as the preservation of size and form is essential for nanoparticle circulation and biodistribution. The absence of crystalline peaks for Toluidine Blue O and lemon extract supports the hypothesis by Wang et al. that organic molecules form a protective layer around the AuNPs, enhancing their biocompatibility and therapeutic potential.

#### *UV-visible Absorption Measurements*

The UV-visible absorption spectra indicated strong interactions between AuNPs and Toluidine Blue O, as evidenced by the shift and broadening of the surface plasmon resonance (SPR) peak. This suggests either nanoparticle aggregation or environmental changes around the nanoparticles, similar to the findings of Robinson-Duggon et al., who observed enhanced optical properties in AuNP-dye interactions, which could be useful in photothermal therapy and biosensing. The extended absorption spectrum of the Au-TB complex compared to pure Toluidine Blue reveals potential for broader-spectrum applications, as noted by Narband et al. in their work on conjugated dyes and AuNPs for biomedical purposes.

#### *Fourier-transform Infrared Spectroscopy (FTIR)*

FTIR analysis confirmed strong interactions between AuNPs and the functional groups of Toluidine Blue O and lemon extract. The presence of hydroxyl, carbonyl, and aromatic groups indicates proper adsorption of organic compounds onto the nanoparticles, enhancing their stability and biocompatibility. This observation is supported by Narband et al., who showed that functional groups stabilize AuNPs and prevent agglomeration. The metal-inorganic vibrations observed in the FTIR spectrum further validate the effective interaction between the gold core and the organic layer, essential for the biological functionality of the nanoparticles, as discussed by Gil-Tomás et al.

#### *Scanning Electron Microscopy (SEM) and Transmission Electron Microscopy (TEM)*

Both SEM and TEM analyses provided important information on the size, shape, and

dispersion patterns of the AuNPs. The lack of intense aggregation, mainly when samples were treated with lemon extract, proved that this extract can provide capping, which stabilizes the nanoparticles. In this respect, Kuo et al. also found that natural extracts affect nanoparticle size and shape, enhancing stability and functionality. Further confirmation of the nanoscale nature of the particles was obtained from TEM images, which showed cubic shapes in the presence of lemon extract-an important factor for ensuring uniform biological responses, according to Vatchalan et al.

#### **CONCLUSION**

The present work represents the study of structural features and elemental composition of gold nanoparticles prepared by Toluidine Blue O dye in combination with lemon extract. These findings showed that AuNPs have a dual role: they have the potential to act like a therapeutic agent when in low amounts, while at higher concentrations, these exhibit toxicity. The partial restoration of pancreatic tissues and stability of AuNPs upon the influence of organic compounds should indicate their perspectives for applications in nanomedicine, first of all for treating diabetes and other chronic diseases. Although this study provides crucial information about therapeutic efficiency and safety, it also calls for further research into the toxicities of AuNPs at high concentrations and their interferences with living tissue. These findings extend existing knowledge in nanotechnology and biomedical science and thus lay the foundation for future studies investigating the therapeutic potential of nanoparticles. The purpose of the research, therefore, is to explain the therapeutic efficacy and safety profiles of nanoparticle-based therapies to assist in the advancement of new applications in nanomedicine.

#### **CONFLICT OF INTEREST**

The authors declare that there is no conflict of interests regarding the publication of this manuscript.

#### **REFERENCES**

1. International Diabetes Federation (IDF). International Year Book and Statesmen's Who's Who: Walter de Gruyter GmbH.
2. WHO Expert Committee on Drug Dependence: Twenty-first report. PsycEXTRA Dataset: American Psychological Association (APA); 1978.

3. Shaw JE, Sicree RA, Zimmet PZ. Global estimates of the prevalence of diabetes for 2010 and 2030. *Diabetes Res Clin Pract.* 2010;87(1):4-14.
4. DeFronzo RA, Ferrannini E, Groop L, Henry RR, Herman WH, Holst JJ, et al. Type 2 diabetes mellitus. *Nature Reviews Disease Primers.* 2015;1(1).
5. Umami AS, Siddiquee S. Nanotechnology Applications in Food: Opportunities and Challenges in Food Industry. *Nanotechnology: Applications in Energy, Drug and Food: Springer International Publishing;* 2018. p. 295-308.
6. Behnia B, Safardoust-Hojaghan H, Amiri O, Salavati-Niasari M, Aali Anvari A. High-performance cement mortars-based composites with colloidal nano-silica: Synthesis, characterization and mechanical properties. *Arabian Journal of Chemistry.* 2021;14(9):103338.
7. Rai M, Yadav A, Gade A. Silver nanoparticles as a new generation of antimicrobials. *Biotechnol Adv.* 2009;27(1):76-83.
8. Ma X, Luan Z, Li J. Inorganic Nanoparticles-Based Systems in Biomedical Applications of Stem Cells: Opportunities and Challenges. *International journal of nanomedicine.* 2023;18:143-182.
9. Dobrovolskaia MA, McNeil SE. Immunological properties of engineered nanomaterials. *Nature Nanotechnology.* 2007;2(8):469-478.
10. Akhtar F, Khan AU, Qazi B, Kulanthaivel S, Mishra P, Akhtar K, et al. A nano phototheranostic approach of toluidine blue conjugated gold silver core shells mediated photodynamic therapy to treat diabetic foot ulcer. *Sci Rep.* 2021;11(1):24464-24464.
11. Yin PT, Shah S, Chhowalla M, Lee K-B. Design, synthesis, and characterization of graphene-nanoparticle hybrid materials for bioapplications. *Chem Rev.* 2015;115(7):2483-2531.
12. Donaldson K, Stone V, Tran CL, Kreyling W, Borm PJA. Nanotoxicology. *Occupational and environmental medicine.* 2004;61(9):727-728.
13. Ramos-Cabrera P, Campos F. Liposomes and nanotechnology in drug development: focus on neurological targets. *International journal of nanomedicine.* 2013;8:951-960.
14. Hajipour MJ, Fromm KM, Akbar Ashkarran A, Jimenez de Aberasturi D, Larramendi IRd, Rojo T, et al. Antibacterial properties of nanoparticles. *Trends Biotechnol.* 2012;30(10):499-511.
15. Vatchalan L, Kesavan B, Selvam P. Adsorption and photocatalytic degradation of auramine-O dye using carbon nanoparticles and Carbon-CaO nanocomposites. *Nanotechnology for Environmental Engineering.* 2022;8(1):109-117.
16. Kitching H, Kenyon AJ, Parkin IP. The interaction of gold and silver nanoparticles with a range of anionic and cationic dyes. *Phys Chem Chem Phys.* 2014;16(13):6050-6059.
17. Hassanpour M, Salavati-Niasari M, Safardoust-Hojaghan H. Sol-gel synthesis and characterization of Co<sub>3</sub>O<sub>4</sub>/CeO<sub>2</sub> nanocomposites and its application for photocatalytic discoloration of organic dye from aqueous solutions. *Environmental Science and Pollution Research.* 2020;28(6):7001-7015.
18. Mohammad-Salehi H, Hamadian M, Safardoust-Hojaghan H. Visible-Light Induced Photodegradation of Methyl Orange via Palladium Nanoparticles Anchored to Chrome and Nitrogen Doped TiO<sub>2</sub> Nanoparticles. *Journal of Inorganic and Organometallic Polymers and Materials.* 2019;29(5):1457-1465.
19. Narband N, Uppal M, Dunnill CW, Hyett G, Wilson M, Parkin IP. The interaction between gold nanoparticles and cationic and anionic dyes: enhanced UV-visible absorption. *Physical Chemistry Chemical Physics.* 2009;11(44):10513.
20. Siddiqi KS, Ur Rahman A, Tajuddin, Husen A. Properties of Zinc Oxide Nanoparticles and Their Activity Against Microbes. *Nanoscale research letters.* 2018;13(1):141-141.
21. Patra HK, Banerjee S, Chaudhuri U, Lahiri P, Dasgupta AK. Cell selective response to gold nanoparticles. *Nanomed Nanotechnol Biol Med.* 2007;3(2):111-119.
22. Akhtar MJ, Ahamed M, Kumar S, Khan MM, Ahmad J, Alrokayan SA. Zinc oxide nanoparticles selectively induce apoptosis in human cancer cells through reactive oxygen species. *International journal of nanomedicine.* 2012;7:845-857.
23. Behnia B, Aali Anvari A, Safardoust-Hojaghan H, Salavati-Niasari M. Positive effects of novel nano-zirconia on flexural and compressive strength of Portland cement paste. *Polyhedron.* 2020;177:114317.
24. Jin X, Zhang M, Dong GS, Xu M, Chen Y, Wang X, et al. Stabilization of face-centered-cubic Mn films via epitaxial growth on GaAs(001). *Appl Phys Lett.* 1994;65(24):3078-3080.
25. Robinson-Duggon J, Mariño-Ocampo N, Barrias P, Zúñiga-Núñez D, Günther G, Edwards AM, et al. Mechanism of Visible-Light Photooxidative Demethylation of Toluidine Blue O. *The Journal of Physical Chemistry A.* 2019;123(23):4863-4872.
26. Rashki S, Dawi EA, Zilaei MR, Safardoust-Hojaghan H, Ghanbari M, Ryadh A, et al. ZnO/chitosan nanocomposites as a new approach for delivery LL37 and evaluation of the inhibitory effects against biofilm-producing Methicillin-resistant Staphylococcus aureus isolated from clinical samples. *Int J Biol Macromol.* 2023;253:127583.
27. Aiken ZA, Hyett G, Dunnill CW, Wilson M, Pratten J, Parkin IP. Antimicrobial Activity in Thin Films of Pseudobrookite-Structured Titanium Oxynitride under UV Irradiation Observed for Escherichia coli. *Chem Vap Deposition.* 2010;16(1-3):19-22.
28. Gil-Tomás J, Tubby S, Parkin IP, Narband N, Dekker L, Nair SP, et al. Lethal photosensitisation of Staphylococcus aureus using a toluidine blue O-tiopronin-gold nanoparticle conjugate. *J Mater Chem.* 2007;17(35):3739.
29. Tian E-K, Wang Y, Ren R, Zheng W, Liao W. Gold Nanoparticle: Recent Progress on Its Antibacterial Applications and Mechanisms. *Journal of Nanomaterials.* 2021;2021:1-18.
30. Safardoust-Hojaghan H, Shakouri-Arani M, Salavati-Niasari M. A facile and reliable route to prepare of lead sulfate nanostructures in the presence of a new sulfur source. *Journal of Materials Science: Materials in Electronics.* 2014;26(3):1518-1524.